Issues in Ice Accretion Aerodynamic Simulation on a Subscale Model

Leia A. Blumenthal,[*] Greg T. Busch,[*] Andy P. Broeren,[†] and Michael B. Bragg[‡]
University of Illinois at Urbana-Champaign, Urbana, IL 61801

This paper presents the results of a study that examined the aerodynamic effects of two important ice-simulation features. It first examines two types of pressure-tap instrumentation, a pressure-slice configuration and a tapped-casting configuration, on streamwise and horn-ice simulations. It then examines the aerodynamic sensitivity of small changes in the geometry of horn-ice simulations. These experiments were carried out using ice simulations from icing-tunnel testing on 18-inch chord NACA 0012 and 23012 models. The subsequent aerodynamic testing was performed at the University of Illinois at Reynolds numbers of 1.0×10^6 to 1.8×10^6 and Mach numbers of 0.10 to 0.18. The results of the first part showed that there were no major differences in integrated aerodynamic performance between the pressure-slice and tapped-casting configurations. Therefore, either method is acceptable provided that care is taken in determining pressure tap placement. The results of the second part showed that small changes in upper-surface horn height and tip radius can significantly affect maximum lift. This is important as it has application to how ice accretions are traced in order to make two-dimensional ice simulations for aerodynamic testing.

Nomenclature

α	= airfoil angle of attack
c	= airfoil chord length
C_d	= drag coefficient
C_l	= lift coefficient
$C_{l,max}$	= maximum lift coefficient
C_m	= quarter-chord pitching-moment coefficient
C_p	= pressure coefficient
k	= ice-shape horn height
M	= freestream Mach number
r	= ice-shape horn tip radius
Re	= freestream Reynolds number, based on the airfoil chord
s	= airfoil model coordinate in surface length
θ	= ice-shape horn angle with respect to the chordline
x	= coordinate in the airfoil model chordwise direction
y	= coordinate normal to the airfoil model chordline
z	= coordinate in the airfoil model spanwise direction

I. Introduction

Due to the extreme degradation in performance under certain icing scenarios, the Federal Aviation Administration (FAA) established a set of icing regulations, including defining the atmospheric conditions for flight into known icing. Manufacturers must go through a process in order to certify aircraft for flying in these conditions. There are various methods currently used to simulate ice accretions for aircraft certification. In some cases a natural ice accretion is analyzed, and in other cases the test uses a simple geometric representation of the ice shape. However, there has not been a comprehensive study performed in the public domain to determine the effect of

---

[*] Graduate Research Assistant, Department of Aerospace Engineering.
[†] Research Scientist, Department of Aerospace Engineering, Senior Member AIAA.
[‡] Professor and Head, Department of Aerospace Engineering, Fellow AIAA.

varying simplifications of the simulation ice shape. In order to properly certify aircraft for flight in icing conditions, the simulation must reasonably represent the ice shape aerodynamically. It is therefore necessary to examine the aerodynamic sensitivity of ice simulations.

A comprehensive simulation test should include ice shapes that would be representative of the majority of possible ice formations. Therefore, a study was performed to determine the differences and similarities between ice accretions.[1] Four classifications of ice shapes were developed—ice roughness, horn ice, streamwise ice, and spanwise-ridge ice. Each of these ice shape types has distinct flowfield physics and consequently different aerodynamic characteristics. It is important to note that there is an overlap region between certain categories and some ice shapes show characteristics of two classifications. The basic flowfield physics and the important characteristics for each of these classifications are discussed in detail in Bragg et al.[1]

Several issues remain to be addressed in order to develop a comprehensive aerodynamic simulation study for ice accretion. For example, it is important to document ice accretion geometry and properly reproduce the accretion in scale. Experimentally, it is important to accurately quantify the flowfield behavior and performance parameters, such as lift and drag. This paper focuses on two of these issues. First the paper examines the different methodologies for measuring pressures on an ice shape; then it examines the sensitivity of simulated ice-shape geometry that may result from the documentation of the ice shape. These are both important factors that directly contribute to the development of a comprehensive simulation strategy.

In order to obtain the aerodynamic data for icing tests, either a force balance is used, pressure taps are placed directly on the ice-shape casting, or a pressure-instrumentation slice is manufactured. The pressure-instrumentation slice is generally designed using a tracing of the ice shape.[2,3,4,5] The coordinates for the tracing are then used to fabricate a thin 2D ice-shape segment in which the pressure taps are placed (Fig. 1). Therefore, the pressure slice is inherently a 2D simulation of the 3D casting. The effect of placing the pressure taps directly in the casting versus using a pressure-instrumentation slice must be understood before the fidelity of such a simulation method can be determined.
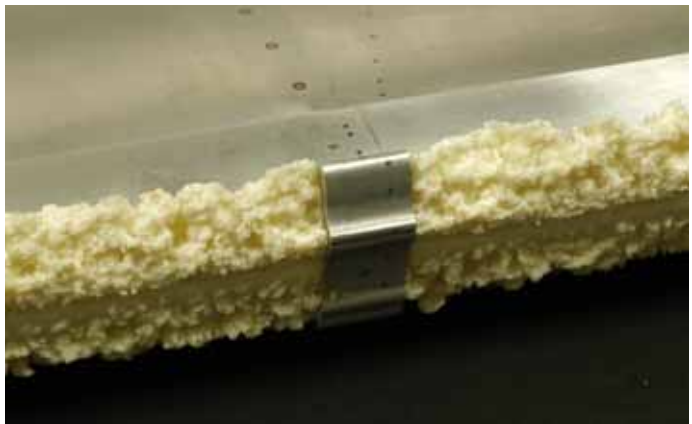
Whether placing pressure taps in the ice shape or in the pressure-slice, the placement of the taps is an important issue when making measurements. Consider a hemisphere on a flat plate simulating a roughness element in a freestream flow. The velocity on the top of the hemisphere is greater than the velocity on the forward or aft face. Therefore, the pressure coefficient (C_p) would be more negative on the top of the hemisphere than either face. Having a greater C_p would affect the integrated lift and drag and could result in inaccurate conclusions if

Fig. 1. Pressure slice installed in a 3D casting of the horn-ice shape used in the horn-geometry sensitivity study.

not properly considered. Previous icing research does not explore this facet of the problem. Of the more recent wind-tunnel tests, the ice shape was not tapped in many cases.[6-9] The studies that do tap the ice shape[10,11] or use a pressure slice[2-5,12] do not explain the methodology for placing the taps on the ice shape or simply placed these taps where the clean taps were located. In a study by Rayle,[13] the placement and geometry of pressure taps located on a smooth surface was shown to affect the measured surface pressure. In addition, when placing the taps in an ice casting, the ice features may interfere with the static-pressure measurements. Early methods of measuring skin friction used an object to partially block the flow around a static-pressure port. In these cases, the static-pressure port would measure a mix of the total and static pressure. This is seen in Stanton tubes, certain configurations of the Preston tube, and in the razor-blade techniques.[14] In the case of ice accretions with highly three-dimensional shapes, the placement of a tap could show a higher or lower pressure than is representative. Therefore, during data analysis these variations must be considered so that pressure variation is not misinterpreted.

The sensitivities in the aerodynamic performance due to geometric changes in the ice shape must also be explored. Simulations of the ice shapes mentioned previously can be made of varying fidelities. The casting of the ice accretion is the highest fidelity and is referred to as a 3D ice shape. A 2D simulation refers to a smoothed extrusion of a tracing from the original casting. The 2D shape has no spanwise variation. Roughness is sometimes added to the 2D simulation in order to increase the fidelity. The lowest fidelity would be a simple geometric shape, such as a quarter-round or a spoiler, simulating the ice accretion.

When making these simplifications it is essential to understand the key flow physics of the ice shape so that important details are not neglected. Since the streamwise and horn-ice shapes were selected for this study, only these will be mentioned. The roughness and spanwise-ridge ice categories are explained in Bragg et al.[1] The aerodynamics of the horn are predominantly determined by a separation bubble resulting from the severe adverse pressure gradients near the tip of the horn. Due to this mechanism, the horn ice generally produces a thin-airfoil type stall. The important characteristics in determining the size and extent of the separation bubble, and thus the performance, are horn height (k/c), tip radius (r/c), angle with respect to the chord line (θ), and the location on the surface (s/c when non-dimensionalized by the chord). Streamwise ice can form a separation bubble, but it is not at a fixed point on the ice shape as in the case of the horn. Depending on the airfoil on which the ice accretes, a short bubble can form instead of a long bubble. With the short bubble, the peak suction will continue to increase up to stall, similar to the clean case. The thickness of the ice at the leading edge and the presence of roughness are also important.

It has been hypothesized that the 3D casting should have a shorter separation bubble than the 2D simulation due to the irregularities in the ice shape acting as vortex generators.[2] The creation of additional vortices increases mixing in the shear layer causing reattachment to occur farther upstream. However, results have been conflicting when tests were performed to compare the 3D castings to the 2D simplifications. In a study by Addy and Chung,[15] a horn-ice shape was tested on an NLF-0414. The 2D ice shape, which was smoothed using 30% control points in SmaggIce,[16] was seen to have a higher $C_{l,max}$ than the 3D ice shape. When a different horn-ice shape and a mixed horn/streamwise-ice shape were tested on a business jet airfoil by Addy et al.,[3] the 2D ice shapes (smoothed using 100% control points) both had a lower $C_{l,max}$ than the 3D ice shapes. In a study by Gurbacki and Bragg[17] performed on a NACA 0012, a third horn-ice shape and a mixed horn/streamwise-ice shape were tested. In this case the 2D horn-ice shape had a lower $C_{l,max}$ than the 3D ice shape whereas the 2D mixed-ice shape had a higher $C_{l,max}$ than the 3D ice shape. Both shapes were smoothed using 50% control points. These results show the importance of selecting the correct simulation when measuring performance. All of these simulations were fabricated based on a tracing of the ice shape. However, when spanwise variation is present on the ice shape the location of the tracing becomes very important. If the horn has a slightly different angle, surface location, radius, or height, then the simulation could yield a different aerodynamic penalty. The differences seen in the studies just mentioned could be a result of the tracing location. Since the 2D model was extruded directly from smoothed versions of the tracing, the 2D simulation of the 3D casting may have slightly different geometric parameters. It is important to note that the measured differences in critical performance, such as $C_{l,max}$, between 2D and 3D ice simulations is small relative to the degradation from the clean case. Nonetheless, it is important for a comprehensive simulation study to understand why these differences exist.

Several studies have already been conducted which parametrically varied horn geometry, but these studies have investigated only large variations in horn height. Kim and Bragg[6] used an NLF-0414 airfoil to simulate three horn heights at various surface locations and with different tip radii. The smallest horn had a height $k/c = 0.0222$ with the taller horns being double and triple this height. Broeren et al.[18] performed a similar test on NACA 23012 and 3415 airfoils. Additionally, Papadakis et al.[19] simulated a horn with height $k/c = 0.0625$ at several surface locations on a NACA 0011. A horn double this size ($k/c = 0.125$) was then tested at the same locations. In all of these tests, horn height was found to be a significant factor in determining the penalty to $C_{l,max}$. However, these studies were intended to evaluate the aerodynamic penalties of various ice shapes. They were not intended to determine the effect of small variations in horn height that could result from differences in quantifying the geometry of a particular ice shape from a tracing.

This paper addresses two relevant issues in the aerodynamic simulation of ice accretions. The first objective was to determine the important factors in pressure measurement and instrumentation. The second objective was to determine the sensitivity of small changes in ice-horn geometry on airfoil performance. During the first study, two variations in the pressure instrumentation technique were analyzed on a streamwise and horn-ice shape. Ice accretions were acquired on an 18-inch chord NACA 23012 airfoil model. Molds of these accretions were used to make castings that were pressure tapped and traced to build a corresponding instrumentation slice. These simulations were then tested in an aerodynamic tunnel on a different 18-inch chord NACA 23012 airfoil model. The horn geometry sensitivity study utilized a pair of 3D castings and 2D-smooth geometries available from previous studies on a NACA 0012 airfoil.[2,17] For the 2D simulations, a new set of horn shapes were developed that parametrically varied the horn height and tip radius. All aerodynamic testing was performed at the University of Illinois' 3×4 ft wind tunnel at $Re = 1.0 \times 10^6$ to 1.8×10^6 and $M = 0.10$ to 0.18.

American Institute of Aeronautics and Astronautics

II. Experimental Methods

The tests performed in this study occurred in the UIUC subsonic, low-turbulence, open-return wind tunnel. The test section was 2.8 ft high, 4 ft wide, and 8 ft long and widened approximately 0.5 inch over the length to account for the growth in the sidewall boundary layer. The inlet contained a four-inch honeycomb followed by four anti-turbulence screens which reduced the empty test-section turbulence intensity to less than 0.1% at all operating speeds for 10 to 5000 Hz bandwidth.[20] The inlet contraction ratio was 7.5:1.

A schematic of the setup is shown in Fig. 2; note that the *z*-coordinate is zero at the model centerline and the *x*-coordinate is zero at the model leading edge. The airfoil model was oriented vertically in the test section. A three-component force balance was used to measure the lift and pitching moment on the airfoil as well as to set the angle of attack. The force balance was located below the test section and supported the model. A traversable wake rake with 25 tubes, measuring both total and static pressure, was used to obtain the airfoil drag. The wake pressures and the model surface pressures were measured with an electronically-scanned pressure system. The lift and moment data presented were taken from both the pressure measurements and the force balance. The drag coefficient was calculated from the wake pressures using standard momentum-deficit methods. The wake drag was measured 4.13-inches above the NACA 23012 model centerline for the pressure-instrumentation portion of the study and was

Fig. 2. Schematic of the wind tunnel configuration.

measured 3.00-inches below the NACA 0012 model centerline for the horn geometry sensitivity portion of the study. More details about this experimental apparatus can be found in Blumenthal.[21]
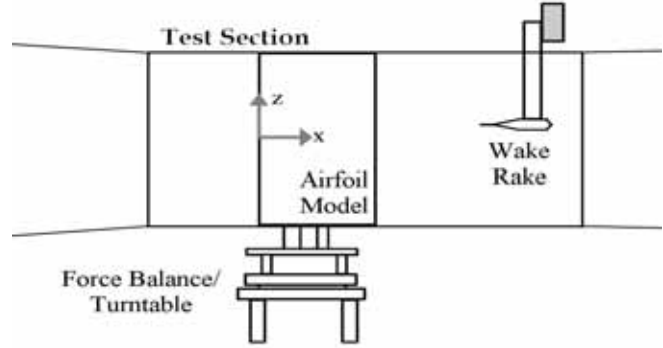
This study also included surface fluorescent oil-flow visualization to study separation bubble lengths, stall mechanisms, and three-dimensional flow features. The amount of fluorescent oil in a particular region on the model is dependent on the local shear stress in that region. The model appears darker in high shear stress reattachment zones or regions of turbulent flow than in low shear stress regions of separated or laminar flow. The method repeated for each run consisted of (1) spraying an even coat of fluorescent oil on the model with an airbrush, (2) running the tunnel for approximately five minutes for the flowfield to reach steady state, and (3) illuminating the fluorescent dye with black lights and documenting the results using digital photography.

All of the aerodynamic coefficients and the angle of attack were corrected for wall interference effects using the methods of Rae and Pope.[22] The experimental uncertainty in these coefficients was estimated using the methods of Kline and McClintock[23] and Coleman and Steele[24] for 20:1 odds. The bias uncertainties in the measured values were calculated from both the surface-pressure and force-balance data (Table 1 and 2). The values were determined by Blumenthal[21] for a horn-ice shape at $\alpha = 3$ deg. with freestream conditions of $Re = 1.8 \times 10^6$ and $M = 0.18$. The uncertainty in estimating the reattachment zone using the surface fluorescent oil-flow visualization technique is estimated to be ± 0.04 x/c.

Table 1. Summary of the Pressure Measurement Uncertainties

Aerodynamic Quantity	Reference Value	Absolute Uncertainty	Relative Uncertainty (%)
C_p	-0.851936	±0.004308	±0.50
C_l	0.452424	±0.002333	±0.52
C_m	0.032785	±0.000414	±1.26
C_d	0.053779	±0.000502	±0.93

Table 2. Summary of the Force-Balance Uncertainties

Aerodynamic Quantity	Reference Value	Absolute Uncertainty	Relative Uncertainty (%)
α	3 degrees	±0.02 degrees	±0.67
C_l	0.457239	±0.002068	±0.45
C_m	0.032203	±0.000116	±0.36

Pressure-Instrumentation Study

The pressure-instrumentation study was performed on a NACA 23012 airfoil, which was an aluminum 18-inch chord, 33.563-inch span model with a removable leading edge. The main body of the model consisted of two chordwise rows of taps and one spanwise row. The primary chordwise row was located at spanwise station $z = 0.50$ inches and the secondary chordwise row was located at $z = -2.80$ inches. The chordwise taps on the model were not swept, as the model was designed for icing applications. Further, the non-swept layout of the pressure taps yielded an additional way to compare spanwise variation. There was also a row of pressure taps oriented spanwise, located at $x/c = 0.70$ on the upper surface. The performance data were acquired through angle-of-attack sweeps. These generally went from negative stall to a few degrees past positive stall in one-degree increments. In cases where several spanwise locations were measured with the wake rake, the angle-of-attack range was reduced.

As discussed in the Introduction, the pressure measured by a tap on an ice shape depends on the exact placement of the tap. To get the best averaged pressure on the ice shape, the taps were placed on varying high and low features so as not to overly bias the integrated values, with all taps being perpendicular to the surface (Fig. 3). Each instrumented section, tapped casting or pressure slice, contained 20 taps. The taps were spaced such that the important flowfield features would be captured. The locations of the taps were based on the coordinates for the pressure slice; thus the locations were approximately in the same place for both configurations. However, in the horn shape, the tap on the tip of the horn was placed in a slightly different location. This was due to the three-dimensional nature of the ice shape. Since the horn thickness varied along the span, it was not possible to place all the pressure tubing for the tapped casting inside the horn. Therefore, pressure tubing was left on the outer surface of the horn on the downstream face. The tubing was placed alongside glaze feathers to limit the effect on the flowfield. This problem did not occur for the streamwise-ice shape and thus all pressure tubing was concealed inside the shape. The comparison of the tapped casting to the pressure slice can be seen in Fig. 4 for the streamwise and horn-ice shapes. The distortion seen in the lower surface of both configurations, but to a much higher extent in the horn-ice shape, was due to a problem in manufacturing the castings. Since the performance of the horn-ice shape is dominated by the upper and lower-surface horns,[1] the modified lower surface should have little effect on the performance as this region would be located in a separation bubble. In addition, since the main objective of this study was to examine the differences between the casting and the pressure-slice configurations, the effect of the lower surface modification was mitigated as the pressure-slice coordinates were based on the casting.

The streamwise ice used in the present study had a stagnation line thickness of approximately 0.58 inches ($k/c = 0.032$). Rime feathers formed on the upper and lower surface of the airfoil to approximately 6% and 17% chord, respectively. The horn ice used in the present study was highly three dimensional and all of the geometric parameters varied along the span. The upper-surface horn had an average height of one inch ($k/c = 0.056$) at an $s/c = 0.01$ with an average angle of 54 degrees with respect to the chord line.
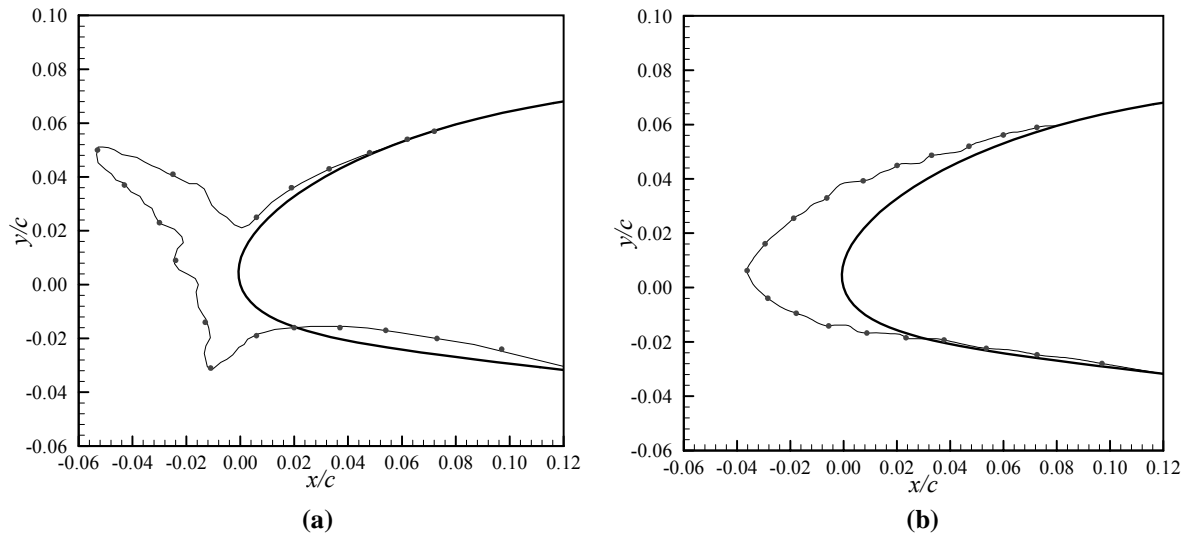

(a)   (b)

Fig. 3. Comparison of the cross-section for the (a) streamwise-ice shape and (b) horn-ice shape. Tap locations are indicated by the filled circles on the ice shape.
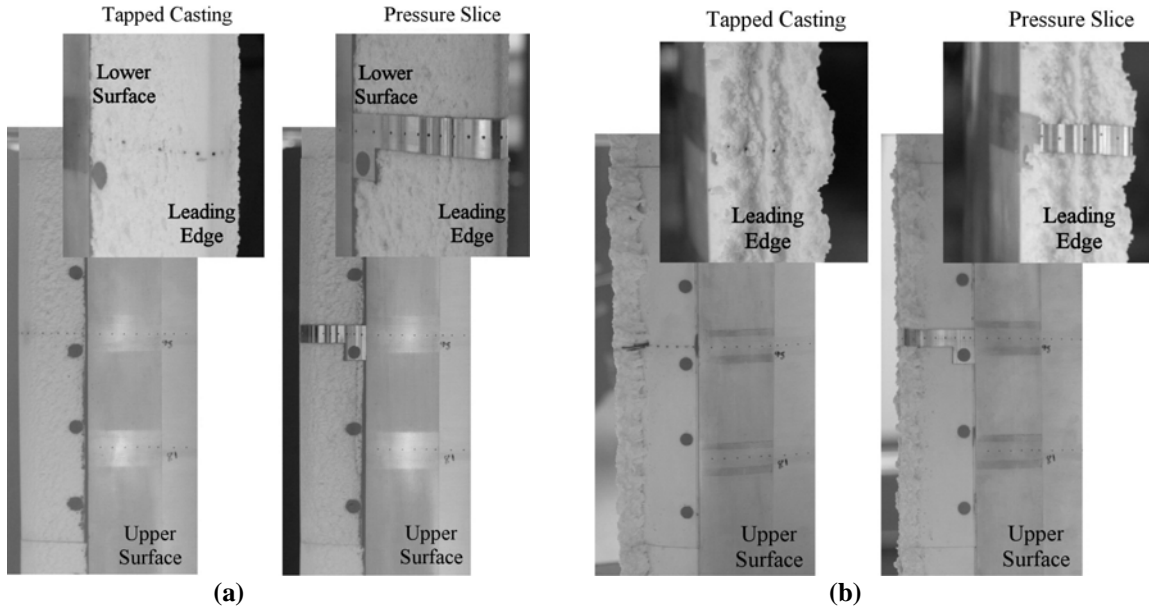
Fig. 4. Comparison of the tapped and pressure-slice configurations for the (a) streamwise-ice shape and (b) horn-ice shape.

Horn-Geometry Sensitivity Study

The model used for the horn-geometry study was an aluminum 18-inch chord, 33.563-inch span NACA 0012 airfoil with a removable leading edge. The clean, un-iced, baseline leading edge could be replaced with several available alternate leading edges with attached simulated ice accretions. On this model, the pressure taps in the main body between the leading edge and mid-chord were swept at approximately 15 degrees from the freestream direction. This model also had a spanwise pressure tap row on the upper surface at 70% chord. More details on the model and simulated ice accretions can be found in Gurbacki.[2]

Both a 3D casting (which used a pressure slice) and a 2D simulation (which was tapped directly) were tested. The 3D casting was produced from a mold of an ice accretion on an 18-inch chord NACA 0012 model in a separate icing test.[17] The 2D simulation was made from a pencil tracing of the 3D casting. The tracing was smoothed using 50% control points in SmaggIce[16] and extruded in the spanwise direction. This simulation had removable upper and lower-surface horns that could be detached individually and replaced by a horn of a different size or shape. These geometries are shown in Fig. 5. The original upper surface horn was about 0.48-inches tall ($k/c = 0.027$) with a tip radius of approximately 0.07 inches ($r/c = 0.0039$) and the original lower surface horn was 0.24-inches tall ($k/c = 0.013$) with a tip radius of 0.24 inches ($r/c = 0.013$). Three upper surface horn modifications were tested. The geometries of these horns were chosen such that they would simulate tracings made at various spanwise stations along the casting. The original tracing appeared to have been made at a high point on the ice shape, so only shorter horn geometries were tested. The first upper surface horn variation was 0.43-inches tall ($k/c = 0.024$, 0.05 inches shorter than the original horn), the second was 0.36-inches tall ($k/c = 0.020$, 0.12 inches shorter than the original horn), and the third was the same height as the original upper surface horn, but had a sharper tip radius, which was 0.02 inches ($r/c = 0.0011$). The $k/c = 0.024$ horn, which will be referred to as the short horn, was chosen such that it would be approximately equal to the mean height of the casting. The very short horn ($k/c = 0.020$) is the same height as the lowest point on the casting. Lower surface horn heights of 0.17 inches ($k/c = 0.009$) and 0.31 inches ($k/c = 0.017$) were also tested, 0.07 inches shorter than and 0.07 inches taller than the original horn, respectively. The lower-surface horn tip radius remained constant ($k/c = 0.013$) for each case. In order to obtain pressure measurements, the 2D simulations were tapped directly.
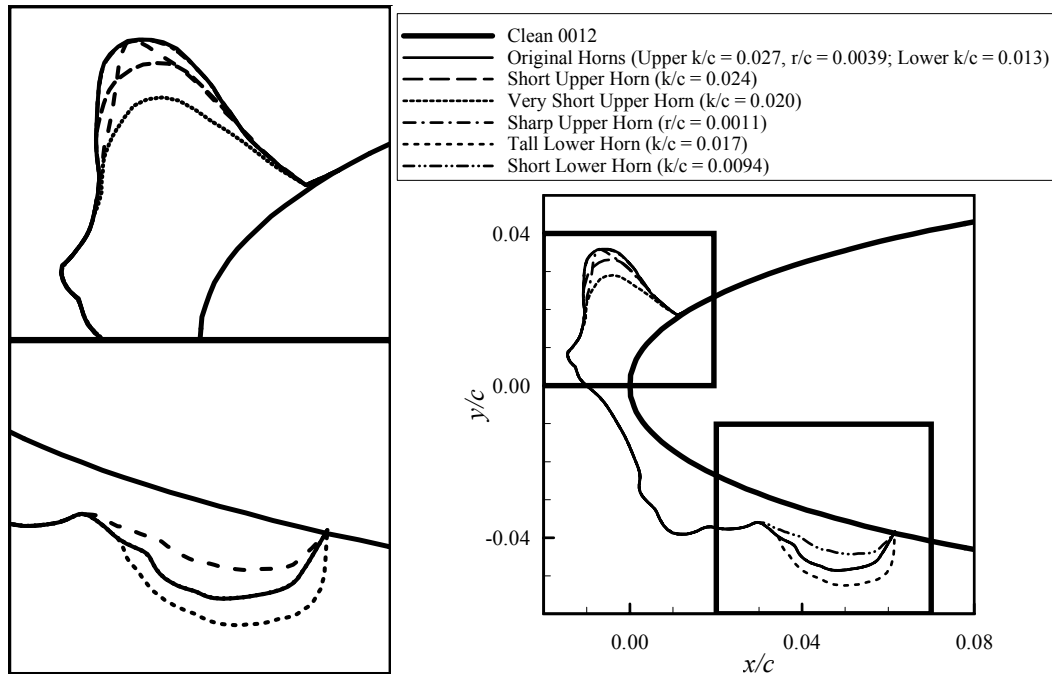
Fig. 5. Parametric variation of horn geometries tested on the NACA 0012 airfoil.

III. Results and Discussion

Since this paper focuses on two significant issues in ice accretion simulation, this section is organized accordingly. The pressure-instrumentation study is discussed first, followed by the horn-geometry sensitivity study. Each section presents the aerodynamic performance results and is followed by a discussion of the important implications.

Pressure-Instrumentation Study

In this study the differences in the measured aerodynamic parameters due to pressure-measurement technique were examined for two ice shapes—a streamwise-ice shape and a horn-ice shape. First the data corresponding to the streamwise-ice shape configurations will be presented followed by the data corresponding to the horn-ice shape configurations.

The performances of the tapped-casting and pressure-slice configurations were very similar to each other for the streamwise-ice shape when compared to the clean configuration (Fig. 6 and Fig. 7). The addition of the streamwise-ice shape caused the airfoil to exhibit a more gradual trailing-edge stall as opposed to the leading-edge stall seen in the clean configuration. However, note that the pressure-slice configuration had a delayed stall when compared to the tapped-casting configuration. This was seen in the data from the integrated pressures as well as that from the force balance. The $C_{l,max}$ was on average reduced by 26% and the α_{stall} was reduced by approximately 2.5 degrees. The drag was increased on average 145% at zero degrees. The tapped casting had both slightly higher lift and higher drag than the pressure-slice configuration, as seen in Fig. 6. This was most likely due to the location where the drag was measured. While the pressure-tap line was located 0.41 inches above the centerline, the drag was measured 4.13 inches above the centerline. Due to the three-dimensional geometry of the ice shape, the drag varied slightly depending on the measurement location (Fig. 8). At 0.41 inches the tapped-casting configuration had a lower drag than the pressure-slice configuration as would be expected by examining the lift curves.
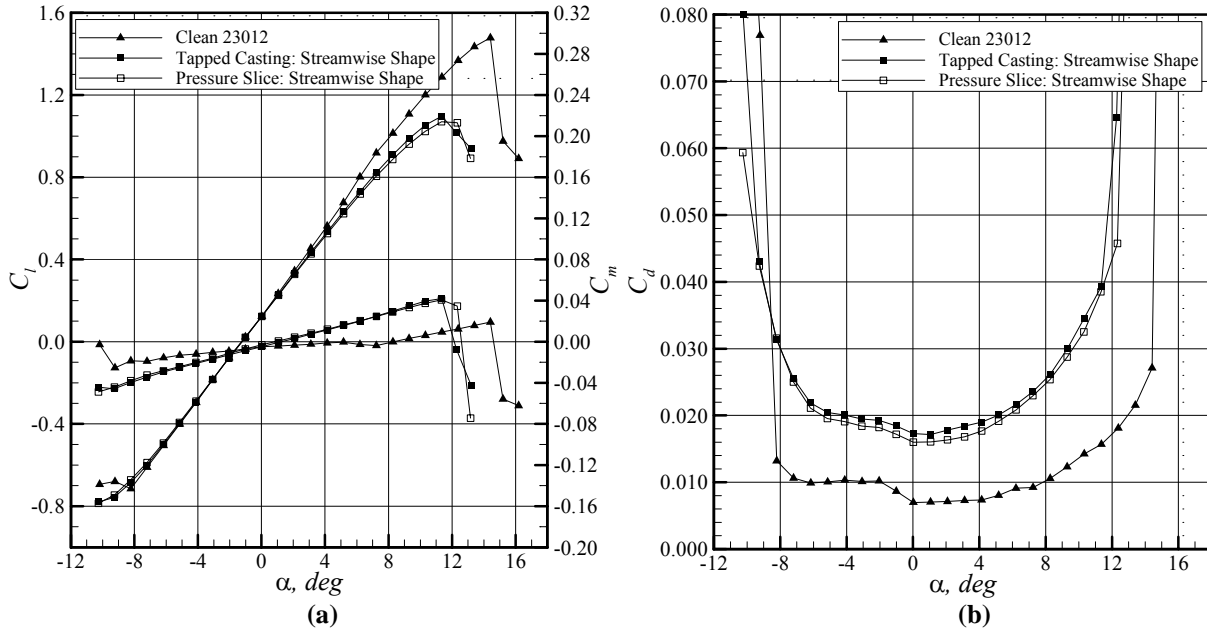
Fig. 6. Comparison of the streamwise-ice configurations for (a) lift and pitching moment and (b) drag. C_l **and** C_m **data are from integrated surface pressures.**
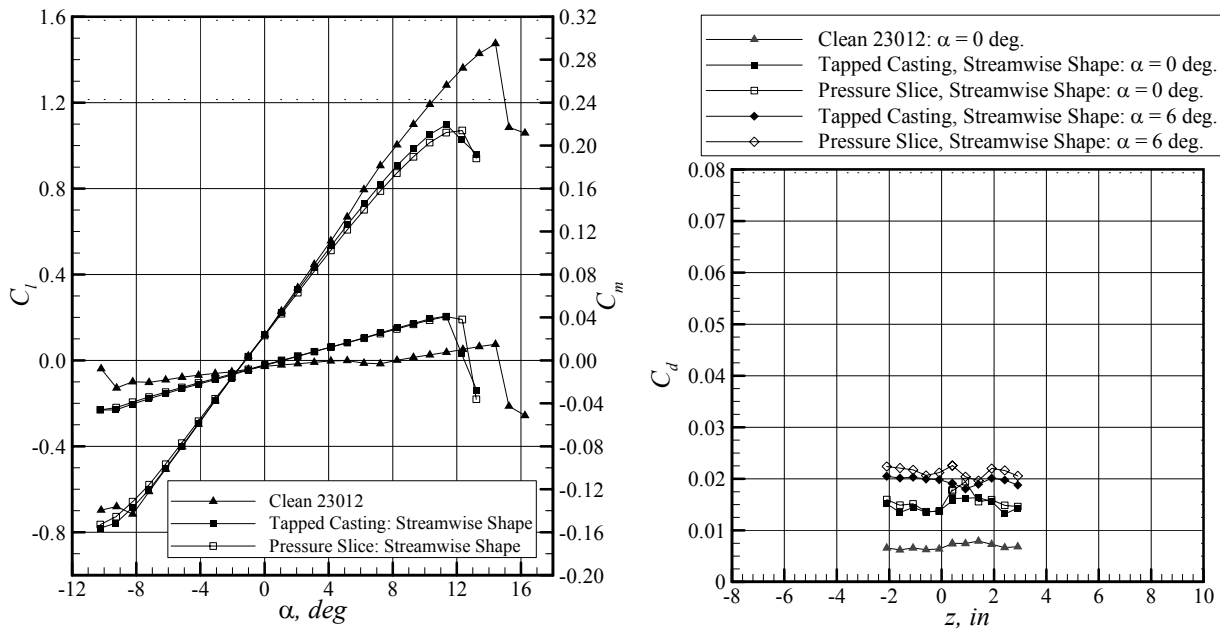

Fig. 7. Comparison of the streamwise-ice configurations for lift and pitching moment calculated from the force-balance data.

Fig. 8. Comparison of the drag measured at several spanwise locations for the streamwise-ice shape for two sample angles of attack.

American Institute of Aeronautics and Astronautics

These differences were also seen in the surface pressures and oil-flow visualization. The pressure distribution at six degrees for the streamwise-ice shape configurations and the clean configuration are shown in Fig. 9. The streamwise-ice shape taps show some variation in the leading-edge region due to the extremely three-dimensional feather features. The pressure taps, while located at the same x/c location, were located at a slightly different location on the feather features of the tapped casting than on the pressure slice. In Fig. 10, the pressure tap locations of the points with a lower magnitude C_p are indicated. From the actual configuration, it is seen that there are feathers just downstream of and in the case of the tapped-casting slightly covering the indicated taps. Therefore, it makes sense that these taps would have a lower velocity and thus a C_p with

Fig. 9. Pressure distribution for the streamwise-ice shape configurations at α = 6 deg.

a lower magnitude based on the earlier analogy of taps on a hemisphere. However, these differences were small, as seen in Fig. 6 and Fig. 7, when the data were integrated to determine lift and pitching moment.
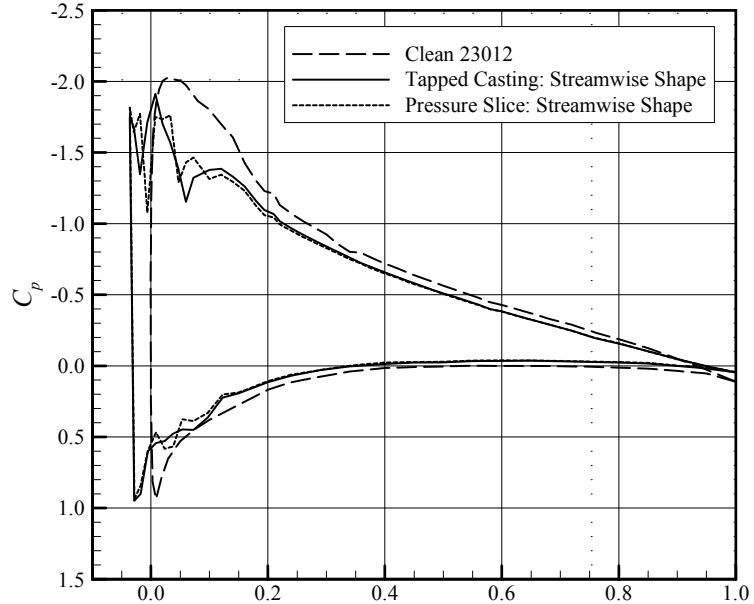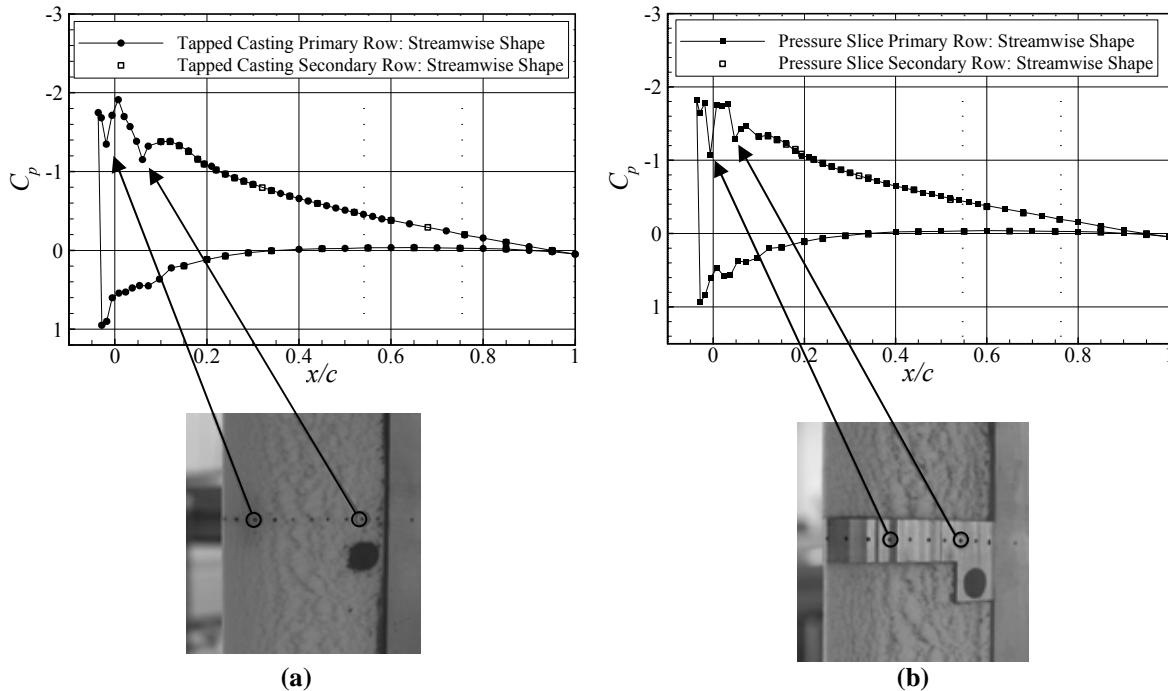

(a)

(b)

Fig. 10. Pressure distribution for the streamwise-ice shape configuration at α = 6 deg. for (a) the tapped-casting configuration and (b) the pressure-slice configuration with distinct pressures indicated.

The fluorescent oil-flow visualization comparison of the tapped-casting and pressure-slice configurations at an angle of attack of 11 degrees is shown in Fig. 11. The direction of the flow is from left to right. The speckles of oil at the trailing edge, which indicate low average shear, further the observation of a trailing-edge stall. The separation location was determined from the airfoil centerline in order to compensate for wall effects due to the floor and

9

ceiling. While the tapped-casting configuration had an estimated separation location of $x/c \approx 0.50$, the pressure-slice configuration was estimated to have maintained attached flow until $x/c \approx 0.57$. While this is close to the estimated uncertainty, the earlier stall was clear during the experiment. Upon stall, the airfoil would start to buffet in the wind tunnel. The tapped-casting configuration consistently began to buffet earlier than the pressure-slice configuration. In a previous study, the flowfield was altered due to the presence of the pressure slice, with vortices forming at the intersections of the pressure slice and ice casting.[2] The present study showed no discontinuity in the flowfield near the pressure-slice region (Fig. 12).

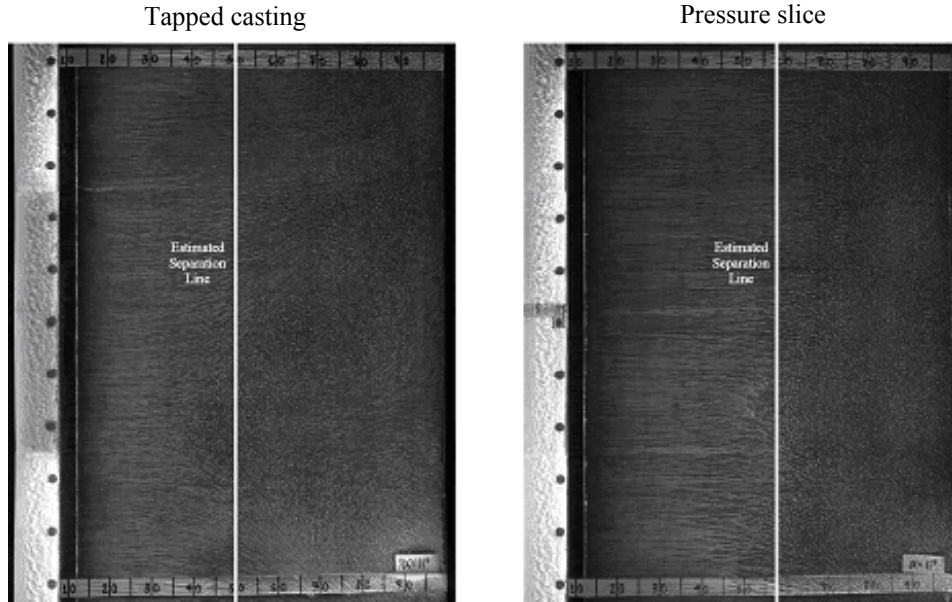Tapped casting   Pressure slice

Fig. 11. Fluorescent oil-flow visualization for the streamwise-ice shape at α = 11 deg. for the tapped-casting and pressure-slice configurations; flow is from left to right.

Tapped casting   Pressure slice
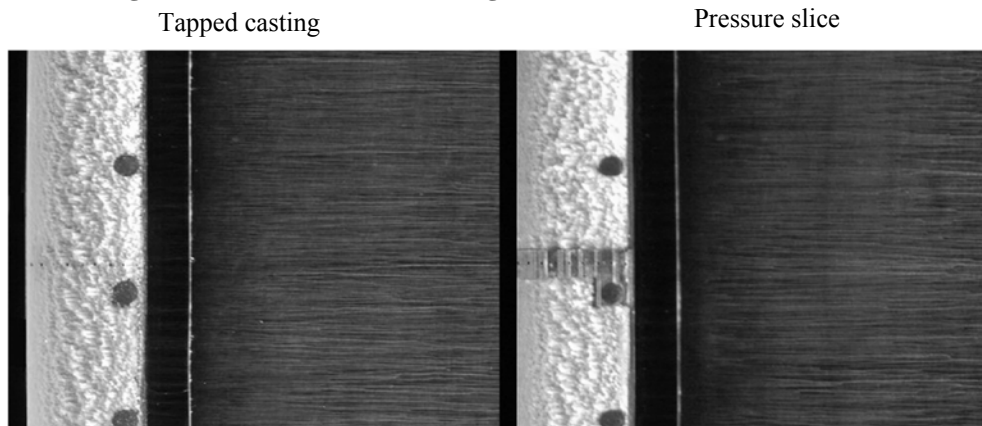

Fig. 12. Close-up of the fluorescent oil-flow visualization for the streamwise-ice shape at α = 11 deg. for the tapped-casting and pressure-slice configurations.

The comparison of the horn-ice configurations for the lift, drag, and pitching moment from the integrated surface pressures is shown in Fig. 13, and the lift and pitching moment from the force-balance data is shown in Fig. 14. No appreciable difference was seen between the tapped-casting and the pressure-slice configurations in the aerodynamic data for either data collection method. The horn-ice configurations showed an average decrease of 61% in $C_{l,max}$ and an eight-degree decrease in α_{stall}. The stall changed from a leading-edge stall in the clean case to a thin-airfoil stall in the iced cases. The drag was greatly increased with a 450% difference at zero degrees when measured at a spanwise location 4.13 inches above the model centerline.
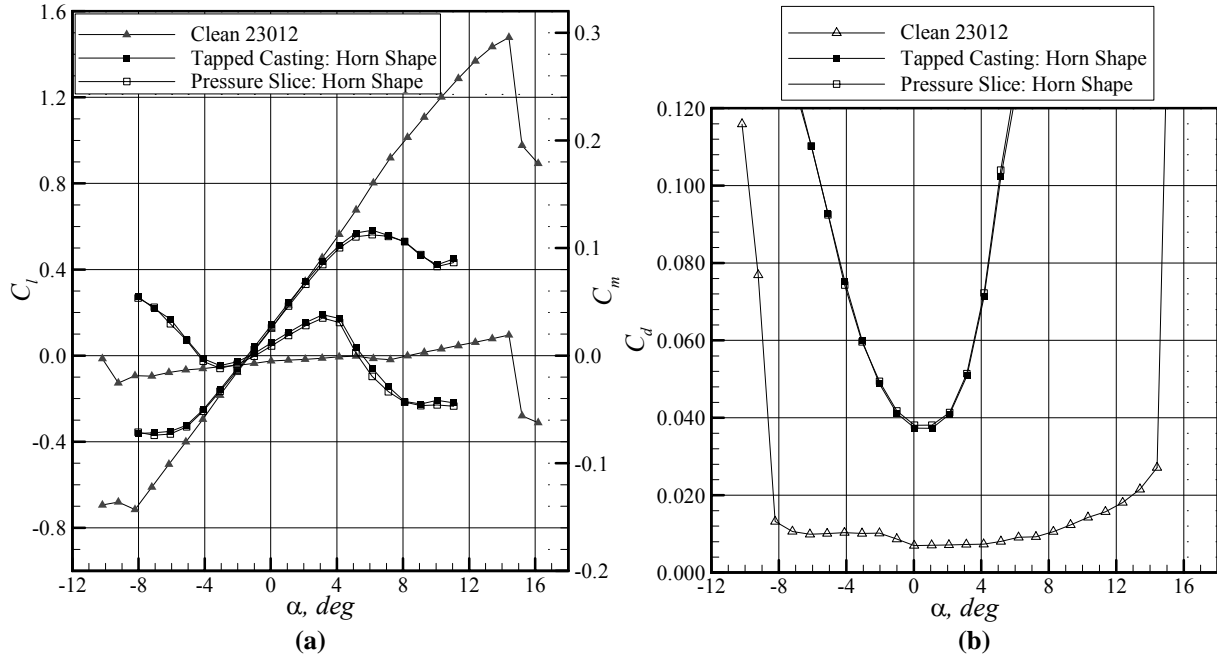
Fig. 13. Comparison of the horn-ice configurations for (a) lift and pitching moment and (b) drag. C_l and C_m data are from integrated surface pressures.

A separation bubble formed due to the horn-ice shape on the upper and lower surface as a result of the adverse pressure gradients caused by the ice-shape geometry. As the angle of attack increased, the upper-surface separation bubble increased in chordwise extent. As the angle of attack decreased, the lower-surface bubble increased in chordwise extent. The pressure distributions for the horn-ice shape configurations and the clean configuration are shown in Fig. 15. The agreement is very good between the tapped-casting and the pressure-slice configurations. This agreement downstream of the horn tip was in part due to the separation bubble. Since the flow was separated, the location and orientation of the pressure taps on the surface geometry played a reduced role in determining the measured pressure. However, in the region forward of the upper-surface horn, a pressure spike is seen in the leading-edge region in the tapped casting that is not evident in the pressure-slice configuration. This difference was due to the tap on the casting being located in a slightly different position than on the pressure slice due to the three-dimensional nature of the ice shape. The pressure tap in the tapped-casting configuration was located at a point in the flowfield where the air was accelerating around the horn geometry before the flow separated. A similar pressure spike is often predicted by computational methods.[25,26]

The separation bubble reattachment location was dependent on the spanwise location (Figs. 16 and 17). The reattachment zone is signified by the low shear region. The approximate reattachment line has been added in white in Fig. 17. To the right of the reattachment line the flow was from left to right and was attached to the surface as it progressed toward the trailing edge. To the left of the reattachment line the flow was reversed and progressed toward the leading edge. No appreciable difference was seen in the oil-flow visualization between the two configurations. Unlike the streamwise-ice shape, neither horn-ice shape configuration showed any indication of a trailing-edge separation. This is consistent with the description of the flowfield given by Bragg et al.[1]
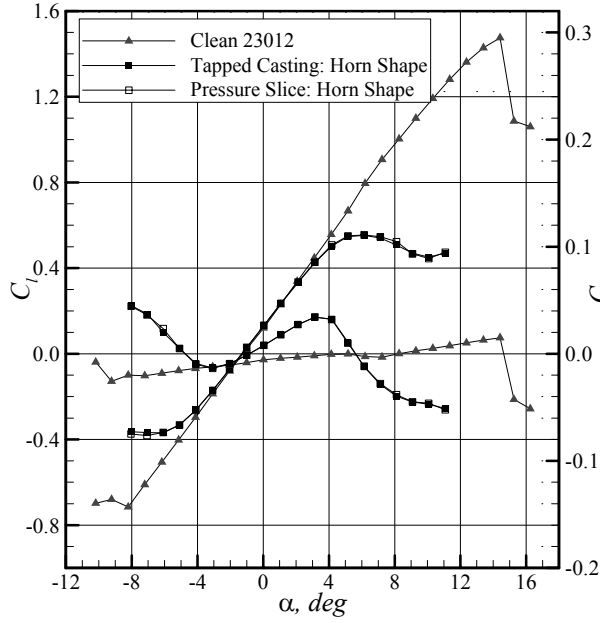
Fig. 14. Comparison of the horn-ice configurations for the lift and pitching moment from the force-balance data.
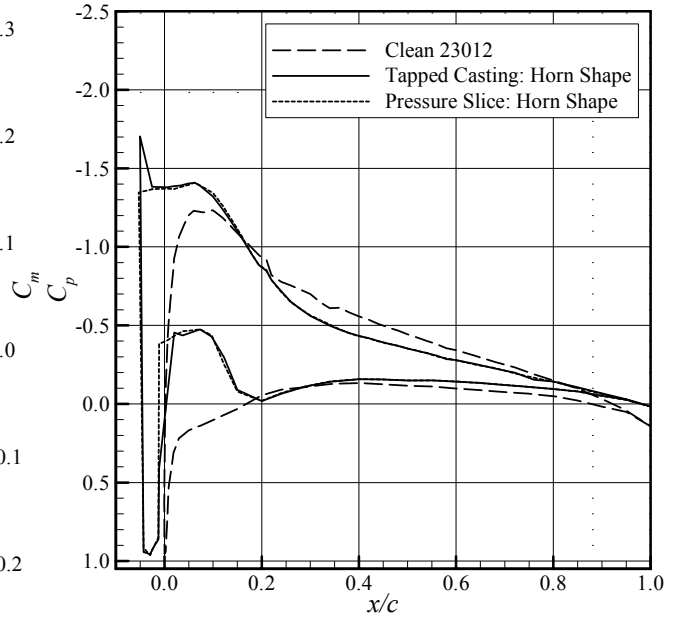

Fig. 15. Pressure distribution for the horn-ice shape configurations at α = 3 deg.
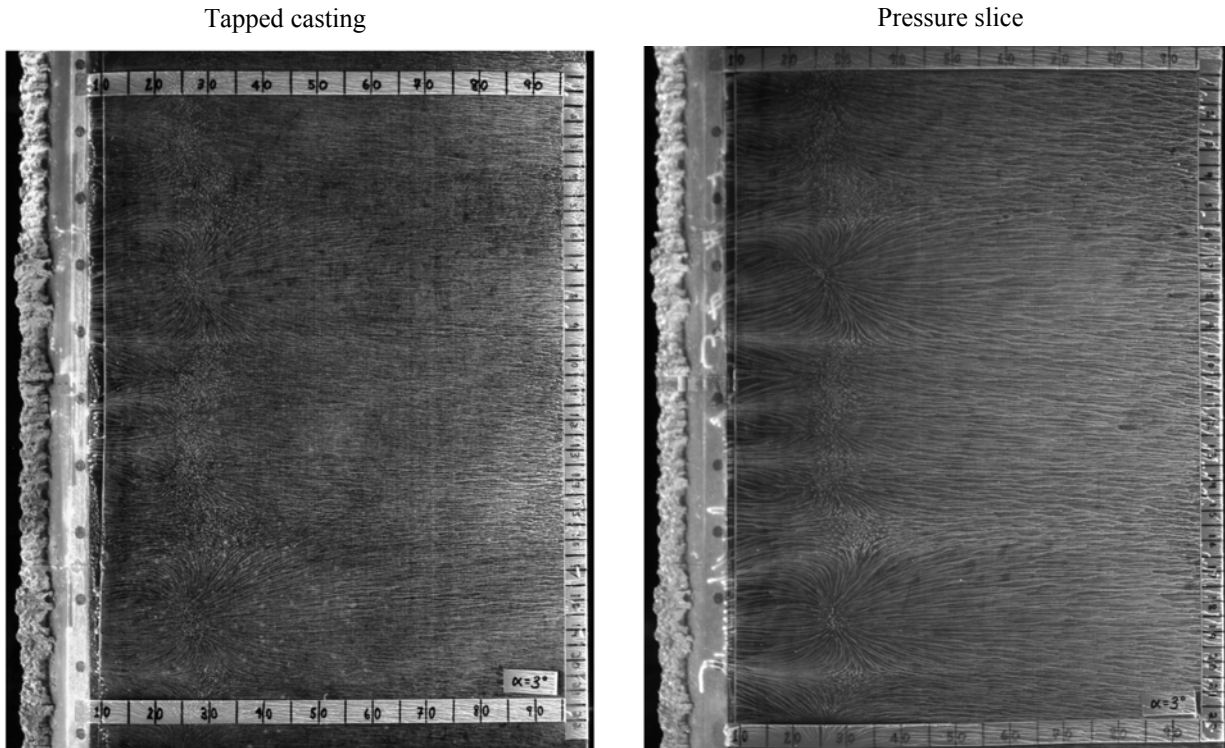
Tapped casting

Pressure slice

Fig. 16. Fluorescent oil-flow visualization for the horn-ice shape at α = 3 deg. for the tapped-casting and pressure-slice configurations; flow is from left to right.

American Institute of Aeronautics and Astronautics

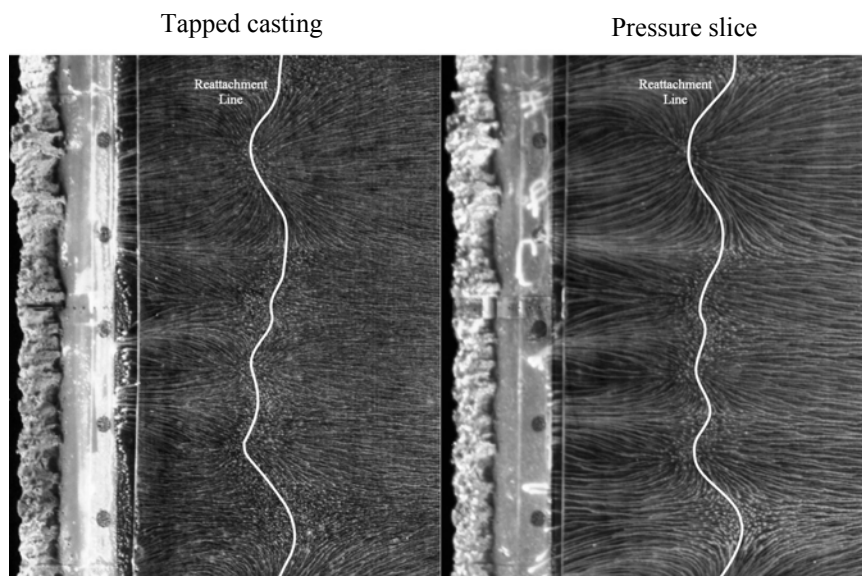Tapped casting   Pressure slice

Fig. 17. Close-up of the fluorescent oil-flow visualization for the horn-ice shape at α = 3 deg. for the tapped-casting and pressure-slice configurations; flow is from left to right.

The drag for the horn-ice shape was clearly dependent on the spanwise location (Fig. 18). These variations were similar in both the pressure-slice and tapped-casting configurations. The reattachment location has also been plotted in Fig. 18. While it seems that the reattachment location is proportional to the drag, more data are needed in order to make any conclusions. When the reattachment position was plotted as a function of the drag, an increasing trend was seen (e.g., if the reattachment location moved further aft, the drag increased). Yet, the measured C_d value is a function of many other factors. For example, when the horn height increases the expectation is that the drag would increase since theoretically the bubble length would increase. However, the drag increased as the horn height decreased as z went from 0.41 to 0.91. The bubble reattachment location, while influenced by the changes in horn height, did not directly correlate to the horn height. This suggests that there are other factors that have an effect on separation bubble size. What is important to note though is that the pressure-slice and tapped-casting configurations were very similar when looking at the aerodynamic performance and the flowfield visualization. Thus both configurations are equally valid for future experiments.
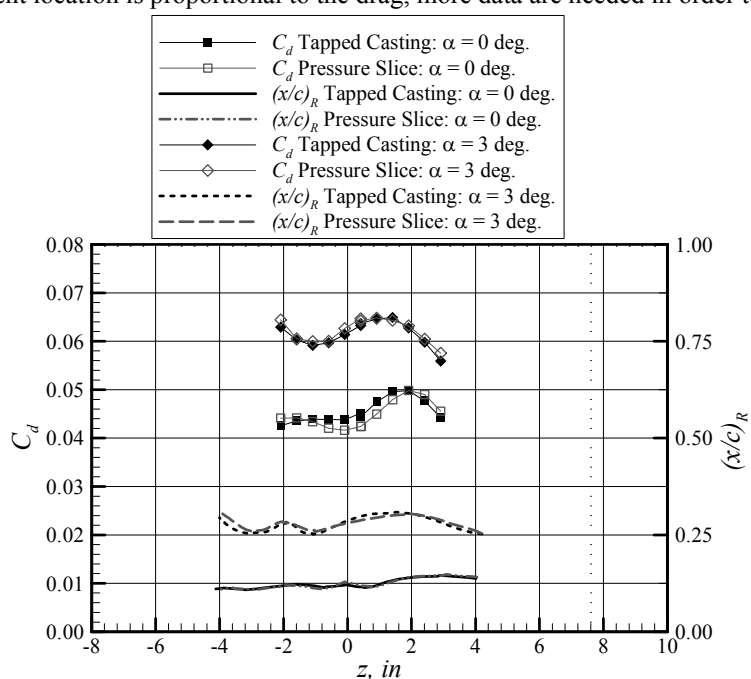
Differences in the aerodynamic

Fig. 18. Comparison of the drag measured at several spanwise locations with the separation bubble reattachment location for the horn-ice configurations.

parameters due to variations in pressure measurement techniques were examined for two ice shapes—a streamwise-ice shape and a horn-ice shape. These data show that at a specified spanwise location, the aerodynamic performance results for a specific ice shape are very similar for both pressure measurement configurations. When the variations

13
American Institute of Aeronautics and Astronautics

were compared across the span of the airfoil, the configurations were also seen to be very similar for each respective ice shape. This was further shown by examining the flowfield using fluorescent oil-flow visualization. Therefore, as long as the pressure taps are placed carefully so as to not bias the results, either configuration can be selected for future experiments.

Horn-Geometry Sensitivity Study

Since both the pressure-slice and tapped-casting configurations yielded nearly identical results for horn-ice shapes, either configuration would have been acceptable for the horn-geometry sensitivity study. The pressure-slice configuration for the casting was used simply because a pressure-slice had already been manufactured and was readily available.

In the parametric horn-geometry study, the upper and lower-surface horn geometries were modified slightly to represent various cross-sections of a three-dimensional horn. The geometries of the horns tested are shown in Fig. 5. The effect of these modifications on $C_{l,max}$, C_m, and C_d were measured to determine if the discrepancy in $C_{l,max}$ between 2D and 3D ice shapes in previous studies might be due to a difference in mean horn geometry.

Both the 3D casting and the 2D simulation exhibited thin-airfoil stall at $\alpha = 7$ deg. The 3D casting had $C_{l,max} = 0.56$ and $C_d = 0.0297$ at $\alpha = 0$ deg. The 2D-smooth simulation with the original horns installed had $C_{l,max} = 0.55$ and $C_d = 0.0248$ at $\alpha = 0$ deg (differences of 2% and 14%, respectively). The difference in drag quickly decreased as the angle of attack increased. At $\alpha = 4$ deg., the difference was only 4%. The presence of roughness on the casting may have caused this difference. As the angle of attack increased, the separation off the tip of the upper-surface horn became more dominant and roughness became less important.

The variations in the upper surface horn height and tip radius considerably affected $C_{l,max}$ and the size of the separation bubble. The effect of modifying the upper-surface horn on the lift, pitching moment, and drag is shown in Fig. 19. The $C_{l,max}$ increased by 7% (with respect to the original 2D simulation) for the short upper-surface horn and increased by 13% for the very short upper-surface horn. Airfoil stall was delayed by one degree for both of the shorter horns. Changes in the height of the upper-surface horn also caused substantial changes in drag. The short horn had 9% less drag and the very short horn had 15% less drag than the original horn (at $\alpha = 0$ deg). This decrease in drag for shorter horn heights became even more noticeable as the angle of attack increased.
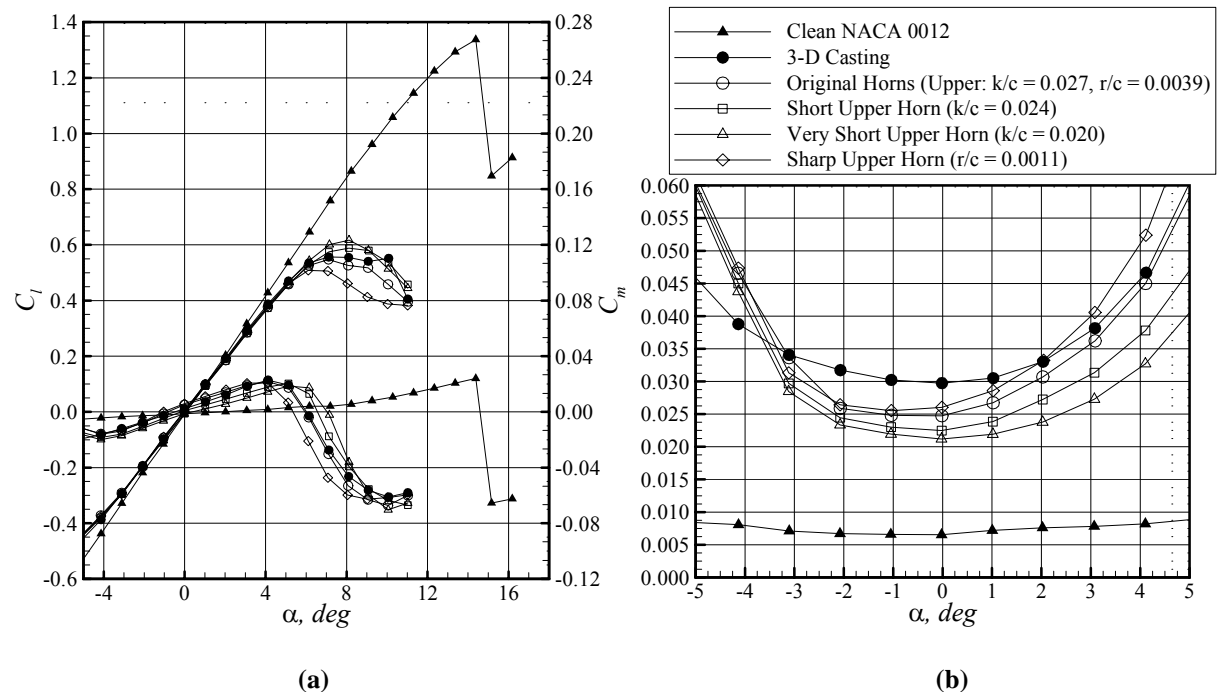

Fig. 19. Comparison of the upper-surface horn variations for (a) lift and pitching moment and (b) drag.

The results for the degradation in $C_{l,max}$ agree with an earlier study by Broeren et al.[18] on NACA 23012, NACA 3415, and NLF-0414 airfoils. The horn height, tip radius, and horn location were each varied parametrically using

simple geometric simulations. The NACA 0012 data from the current study is superimposed on the data from the previous study in Fig. 20 (the horn was located at $s/c = 0.020$ on the NACA 0012 and at $s/c = 0.017$ on the other three airfoils). The differences in $C_{l,max}$ due to changes in horn height were consistent for the NACA 0012 and NACA 23012; the penalty to these airfoils was likely similar because they both derive their lift mainly from a large suction peak near their leading edges. The NACA 3415 and NLF-0414 were less affected by the ice shape because they are more uniformly loaded.[18]

Decreasing the upper-surface horn tip radius also affected $C_{l,max}$, decreasing it by 8% and causing stall to occur one degree earlier. This contrasts with an earlier parametric study using simple geometric shapes on an NLF-0414 in which changes in the upper-surface horn tip radius affected $C_{l,max}$ by only 1%.[27] On the NLF-0414, the horn tip radius was varied from 1.10% to 0%, whereas the tip radius of the shape on the NACA 0012 was varied from 0.39% to 0.11%. A smaller change in tip radius had a larger effect on the $C_{l,max}$ of the NACA 0012. This suggests that some airfoil and ice shape geometries are more sensitive to horn tip radius than are others. The sharp upper-surface horn had a $C_d = 0.0260$ at $\alpha = 0$ deg, an increase of only about 5%. As the angle of attack increased, the difference in drag between the sharp and original horn cases became larger. By $\alpha = 4$ deg. the difference in drag grew to 16%.

The pressure distributions around the airfoil for each of the upper-surface horns at $\alpha = 4$ degrees are shown in Fig. 21. The differences in lift and drag seen in Fig. 19 can be explained by the relative sizes of the separation bubble that formed immediately downstream of the horn. A plateau of relatively constant pressure is indicative of a

Fig. 20. Comparison of results between the current study and a previous study by Broeren et al.[18]

separation bubble and can be used in conjunction with the clean pressure distribution to estimate the reattachment location. The intersection of the iced and clean airfoil pressure distributions is the approximate reattachment location,[28] although recent studies have shown reattachment may occur a few percent chord beyond this intersection.[2,21] The original ice shape had a pressure spike near the leading edge where the flow accelerated around the tip of the horn. This spike was followed by a separation bubble that extended from the tip of the horn ($x/c \approx -0.005$) to $x/c \approx 0.23$. The separation bubble for the 3D casting was nearly identical. However, the 3D casting and other upper-surface horn geometries did not exhibit the pressure spike near the leading edge because this region of low pressure was localized and the taps were in slightly different locations on the horn due to the differing geometries. The sharp upper-surface horn had the largest separation bubble, reattaching to the airfoil at $x/c \approx 0.32$. The very short upper-surface horn ($k/c = 0.020$), had the smallest separation bubble, reattaching at $x/c \approx 0.14$. The very short upper-surface horn had the lowest drag at $\alpha = 4$ deg., corresponding to the smallest bubble. Additionally, it stalled later and had a higher $C_{l,max}$ than the original horn case.
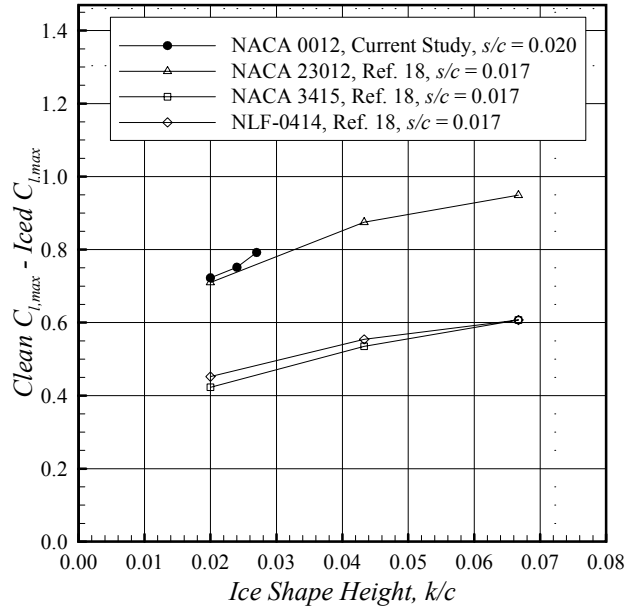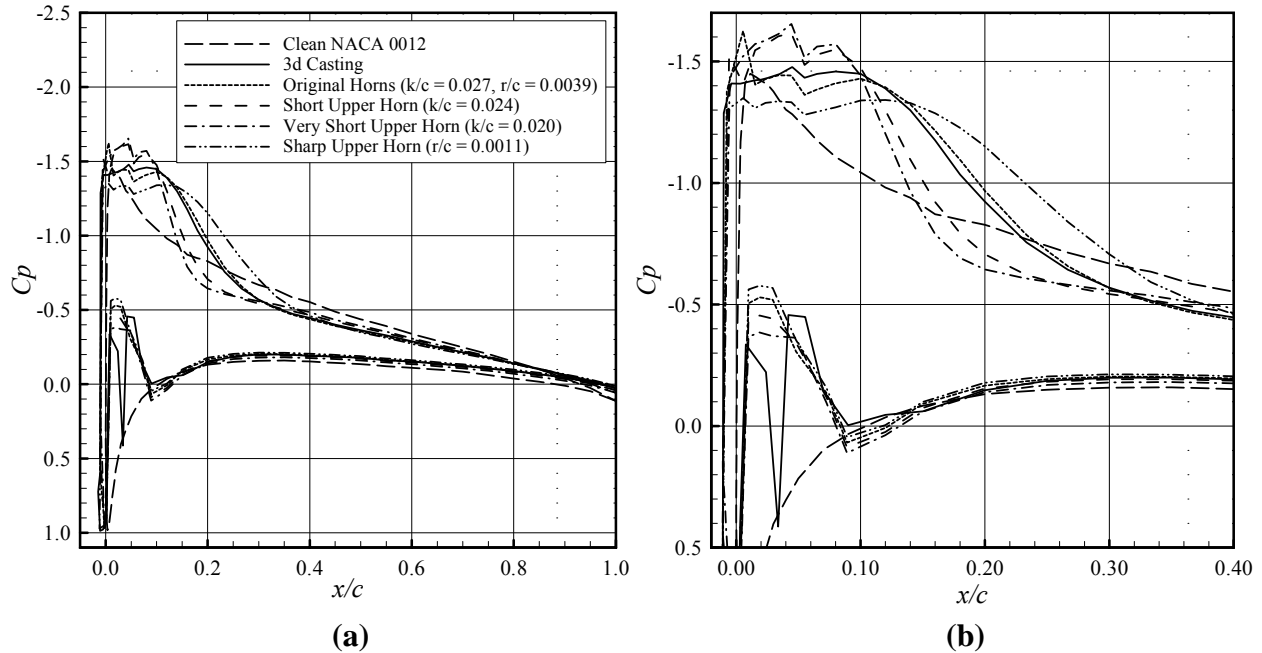
Fig. 21. (a) Full and (b) detail pressure distributions for various upper-surface horn geometries at $\alpha = 4$ deg.

The effects on lift, pitching moment, and drag due to modifying the lower-surface horn height are shown in Fig. 22. All data presented for the lower-surface horn variations are with the original upper-surface horn at $Re = 1.0 \times 10^6$ and $M = 0.10$. Altering the lower-surface horn height had little effect on $C_{l,max}$. The variations in drag due to changes in lower-surface horn height were on the same order as the variations when the upper-surface horn height was altered. The original lower-surface horn configuration had $C_d = 0.0244$ at $\alpha = 0$ deg, 6% lower than the tall lower-surface horn and 24% lower than the short lower-surface horn. The drag for each configuration converged as the angle of attack increased past zero because features on the lower surface became less important at high positive angles of attack. At negative angles of attack, the tall lower-surface horn surprisingly had the lowest drag. This was most likely due to the presence of a protrusion on the ice shape in front of the lower-surface horn.

This apparent anomaly in C_d can be further explained by examining the pressure distributions for each lower-surface horn variation (Fig. 23). These distributions show a pressure plateau on the lower surface beginning at $x/c \approx$ 0.01 ($\alpha = -2$ deg), revealing that the flow separated off a protrusion in front of the lower-surface horn (Figs. 5 and 23). For the original and short lower-surface horns, the flow reattached to the main airfoil at $x/c \approx 0.18$ and $x/c \approx$ 0.20, respectively. The tall lower-surface horn, on the other hand, was considerably larger than the protrusion and mitigated its effects. The initial separation bubble from the protrusion was much smaller than for the other cases, and the flow reattached to the tall lower-surface horn and then separated a second time. The second reattachment location occurred on the main airfoil surface near $x/c \approx 0.12$, farther upstream than the separation bubble for the short and original lower-surface horn cases. The separation bubble for the 3D casting was also shorter than for the short and original lower-surface horn cases. The protrusion was not located directly in front of the row of taps, but rather it was located just beside the taps. This reduced its effect, so the flow reattached to the lower-surface horn. The flow then separated again off the horn and reattached at $x/c \approx 0.13$. Conversely, the short and original horns, which were not significantly larger than the initial protrusion, were too short to provide a point of reattachment. There was no chance for a second separation bubble to form for these cases. The tall lower-surface horn had the lowest drag at negative angles of attack because it had two small separation bubbles instead of one large separation bubble. As α increased toward zero degrees, the flow reattached to the original horn, cutting the large separation bubble into two smaller bubbles for this case as well. When this occurred (at $\alpha = -1$ deg.), the drag of the original lower-surface horn dropped below that of the tall lower-surface horn because the separation bubbles of the original
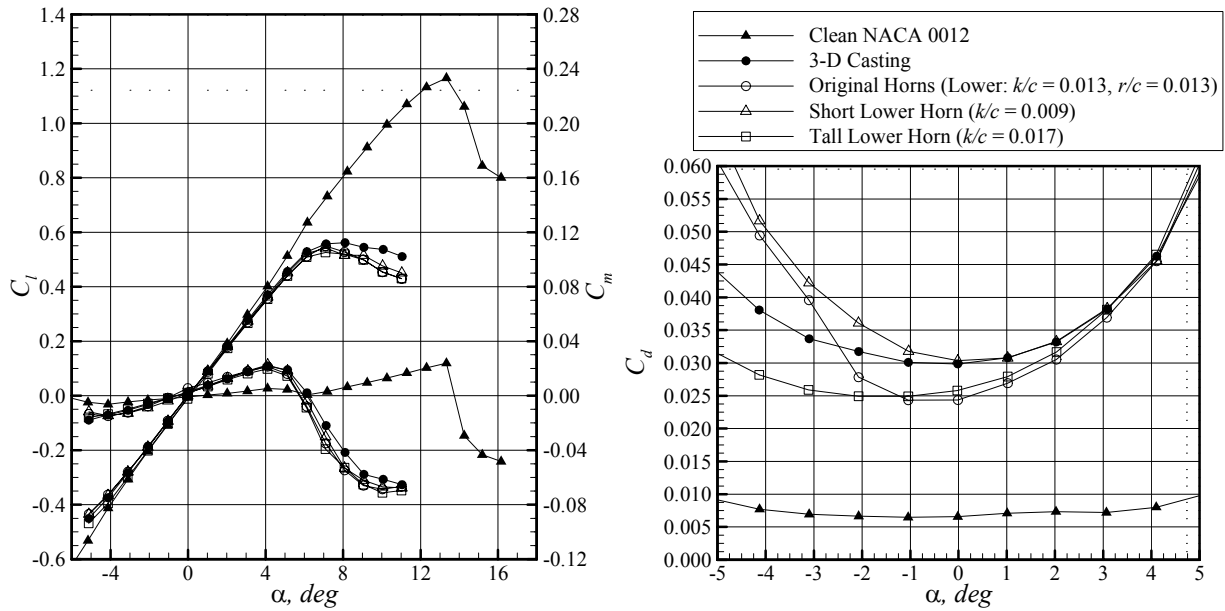
16
American Institute of Aeronautics and Astronautics

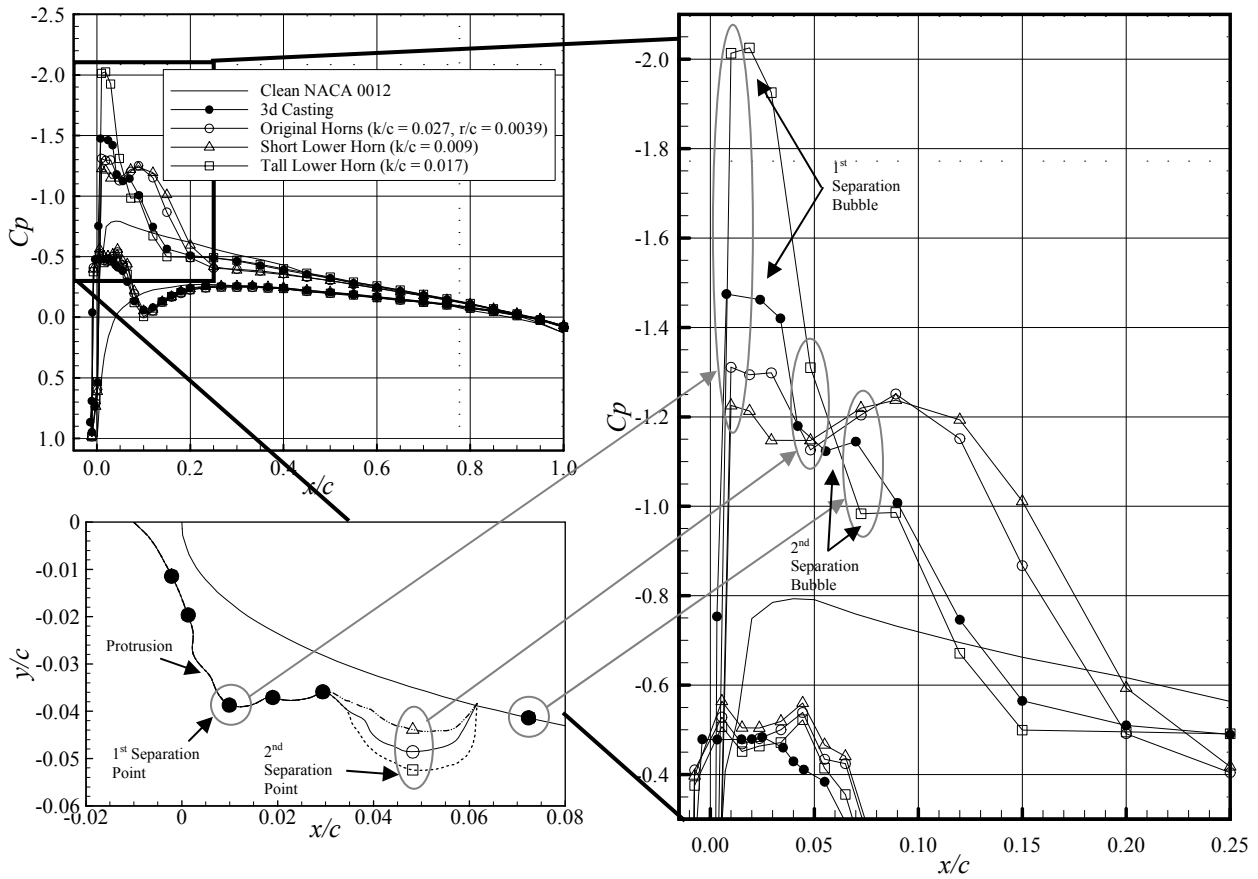**Fig. 22. Comparison of the lower surface horn variations for (a) lift and pitching moment and (b) drag.**

Fig. 23. Pressure distributions for lower surface horn geometries at α = -2 deg.

horn were smaller than the bubbles of the tall horn. As α continued to increase, the separation bubble from the initial protrusion became less important, so the drag coefficients for each case converged. The lift was not significantly different between the three cases because lift is relatively insensitive to separation bubbles until the airfoil is near stall. These data suggest that ice shapes with short lower-surface horns may have other features that have a significant effect on the flowfield along the lower surface of the airfoil.

It was stated earlier that the tracing used to extrude the 2D simulation appeared to have been made at a high point on the ice shape. This would cause the corresponding $C_{l,max}$ to be slightly lower than that of the 3D casting. Additionally, the tracing was made with the pencil held vertically which might cause the tip radius of the horn to be slightly enlarged for the 2D simulation, thus yielding a higher $C_{l,max}$. This study demonstrated that a decrease in horn height of 11% could increase $C_{l,max}$ by 7% and a sharp tip radius instead of a rounder radius could decrease $C_{l,max}$ by 8%. Recall that the difference in $C_{l,max}$ between the 3D casting and the 2D simulation was 2%. This 2% difference was likely due to the 2D simulation having some combination of a taller horn and slightly larger tip radius.

The difference between the 3D casting and the 2D simulation in drag was more likely due to the presence of roughness on the casting than a disparity in mean geometric features. At α = 0 deg. the difference in drag was 16% and at α = 4 deg. the difference was 4%. The drag converged as angle of attack increased, suggesting that the reason for the difference in drag at α = 0 deg. was due either to a discrepancy in geometry on the lower surface or to roughness. The lower-surface horn on the 2D simulation appeared to be representative of the lower-surface horn on the 3D casting, so it is more likely that the roughness of the casting caused the extra drag. Additionally, another study on the same ice shape showed that the presence of 14 grit roughness along the front surface of the ice shape increased drag at α = 0 deg. by 24% (Fig. 24). This accounts for the higher drag of the 3D casting.

The large variations in $C_{l,max}$ and drag resulting from small variations in upper-surface horn height and tip radius suggest that tracings of an ice shape must be made carefully. The location of the tracing must be

Fig. 24. Effect of roughness along the front surface of the original 2D simulation.

chosen at a cross-section that is representative of the entire ice shape. If the tracing is made at a high point on the ice shape, the 2D extrusion of that ice shape will likely have a lower $C_{l,max}$ and higher C_d than the corresponding casting. Additionally, the tip of the upper-surface horn must be traced with the pencil tip held as closely as possible to the shape to prevent the horn from having an unrepresentatively large tip radius. The focus should be placed on selecting the best location for the upper-surface horn tracing as variations in lower-surface horn height had a much smaller effect on the $C_{l,max}$ than did variations in upper-surface horn height. If possible, several tracings should be averaged together to form a single tracing that is more representative of the ice accretion.
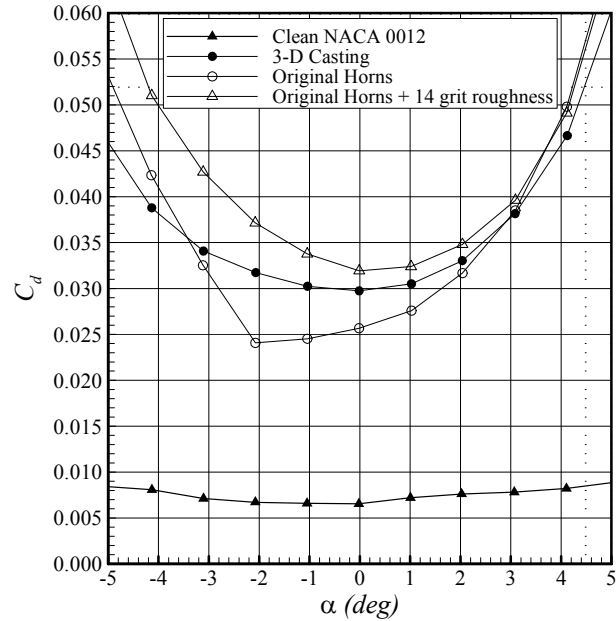
IV. Summary and Conclusions

The objectives of this study were to understand the important factors in pressure instrumentation on simulated ice shapes and the sensitivity to small changes in simulated ice-shape geometry. The ice castings used in this study were made from molds of ice accreted in an icing wind tunnel, and the 2D-smooth extrusions were generated from tracings of ice accreted in an icing wind tunnel. The aerodynamic performance tests and oil-flow visualization were performed at the UIUC 3×4 ft wind tunnel at $Re = 1.0\times10^6$ to 1.8×10^6 and $M = 0.10$ to 0.18.

For the pressure-instrumentation study, two ice shapes were selected—a streamwise-ice shape and a horn-ice shape. Each shape was tested in the tapped-casting configuration, where pressure taps were placed directly into the ice shape, and in the pressure-slice configuration, where an instrumentation piece was manufactured based on tracings of the ice casting. Each ice shape caused large performance degradations compared to the clean airfoil, and the differences seen between the tapped-casting and pressure-slice configurations for each shape were small compared to these degradations. In both configurations the addition of the ice shape yielded the typical results for a

American Institute of Aeronautics and Astronautics

NACA 23012—the streamwise-ice shape induced a trailing-edge stall and the horn-ice shape induced a thin-airfoil stall. However, it is important to note that when the streamwise-ice shape was tested, differences were seen between the tapped-casting and the pressure-slice configurations near stall. In the pressure-slice case, the flowfield remained attached slightly longer than in the tapped-casting case. No appreciable difference was seen between either of the horn-ice shape configurations. Unlike the streamwise shape, the drag for the horn-ice shape was highly dependent on spanwise location. However, these variations were similar for both the pressure-slice and tapped-casting configurations. The location of the tap placement was seen to be important when the surface-pressure distributions were examined. Therefore, regardless of whether a tapped casting or pressure slice is used, the determination of tap location should be done with care. Further, either configuration can be selected for future experiments as both showed such similar results.

The purpose of the horn-geometry sensitivity study was to consider what variations in a 2D simulation could result from making an ice shape tracing at an unrepresentative location (e.g., at an unusually low or high point) on the ice accretion and to quantify the aerodynamic effects of these variations on an airfoil with a 2D ice shape simulation. A horn-ice simulation was constructed that had removable upper and lower-surface horns. The $C_{l,max}$ of the 2D simulation was 2% lower than the $C_{l,max}$ of the 3D casting, and the C_d of the 2D simulation at $\alpha = 0$ deg. was 14% lower than that of the 3D casting. Shortening the upper-surface horn of the 2D simulation by $k/c = 0.007$ resulted in an increase in $C_{l,max}$ of up to 13% and a decrease in C_d at $\alpha = 0$ deg. of up to 15%. Sharpening the upper-surface horn caused a decrease in $C_{l,max}$ of 8% and an increase in C_d, especially at high angles of attack. Varying the lower-surface horn height did not significantly affect $C_{l,max}$, though it did cause changes in C_d at negative and low angles of attack. The penalties to $C_{l,max}$ and C_d were directly related to the size of the separation bubble resulting from the horn.

These results demonstrate the sensitivity in iced airfoil performance to small changes in geometry and the need to carefully choose a representative 2D ice shape. For cases when an ice tracing is used, care must be taken to select a location that is representative of the entire ice shape. In particular, special attention should be paid to the upper-surface horn since small variations will cause considerable changes in $C_{l,max}$ and C_d. The lower-surface horn is less significant. Small variations make a difference only in C_d, and only at low angles of attack. Furthermore, the tip of the upper-surface horn should be traced closely so that the tip radius is not artificially enlarged. Ice-shape roughness is also important in measuring C_d at low angles of attack, but its effect diminishes as the angle of attack increases. Therefore, if the upper-surface horn height and tip radius are accurately captured in the tracing of the ice shape, then $C_{l,max}$ and C_d at positive angles of attack can be modeled reasonably well with a 2D-smooth extrusion of the ice shape.

References

[1] Bragg, M. B., Broeren, A. P., and Blumenthal, L. A., "Iced-Airfoil Aerodynamics," *Progress in Aerospace Sciences*, Vol. 41, No. 5, July 2005, pp. 323-418.

[2] Gurbacki, H. M., "Ice-Induced Unsteady Flowfield Effects on Airfoil Performance," Ph.D. Dissertation, Dept. of Aeronautical and Astronautical Engineering, Univ. of Illinois, Urbana, IL, 2003.

[3] Addy, Jr., H. E., Broeren, A. P., Zoeckler, J. G., and Lee, S., "A Wind Tunnel Study of Icing Effects on a Business Jet Airfoil," AIAA Paper 2003-0727, 41st Aerospace Sciences Meeting and Exhibit, Reno, NV, Jan. 2003.

[4] Addy, Jr., H. E., and Chung, J. J., "A Wind Tunnel Study of Icing Effects on a Natural Laminar Flow Airfoil," AIAA Paper 2000-0095, 38th Aerospace Sciences Meeting and Exhibit, Reno, NV, Jan. 2000.

[5] Broeren, A.P., Bragg, M.B., and Addy, H.E., Jr., "Effect of Intercycle Ice Accretions on Aerodynamic Performance," *Journal of Aircraft*, Vol. 41, No. 1, Jan.-Feb. 2004, pp. 165-174.

[6] Kim, H. S., and Bragg, M. B., "Effects of Leading-Edge Ice Accretion Geometry on Airfoil Performance," AIAA Paper 99-3150, 17th Applied Aerodynamics Conference, Norfolk, VA, June 1999.

[7] Lee, S., "Effects of Supercooled Large-Droplet Icing on Airfoil Aerodynamics", Ph.D. Dissertation, Dept. of Aeronautical and Astronautical Engineering, Univ. of Illinois, Urbana, IL, 2001.

[8] Papadakis, M., Yeong, H. W., Wong, S.-C., Bargas, M., and Potapczuk, M. G., "Aerodynamic Performance of a Swept Wing with Ice Accretions," AIAA Paper 2003-0731, 41st Aerospace Sciences Meeting and Exhibit, Reno, NV, Jan. 2003.

[9] Jackson, D. G., and Bragg, M. B., "Aerodynamic Performance of an NLF Airfoil with Simulated Ice," AIAA Paper 99-0373, 41st Aerospace Sciences Meeting and Exhibit, Reno, NV, Jan. 1999.

[10] Papadakis, M., Yeong, H. W., Chandrasekharan, R., Hinson, M., Ratvasky, T. P., and Giriunas, J., "Experimental Investigation of Simulated Ice Accretions on a Full-Scale T-Tail," AIAA Paper 2001-0090, 39th Aerospace Sciences Meeting and Exhibit, Reno, NV, Jan. 2001.

[11] Gregorek, G., Dreese, J. J., and Noé, K. L., "Additional Testing of the DHC-6 Twin Otter Tailplane Iced Airfoil Section in the Ohio State University 7×10 Low Speed Wind Tunnel," NASA/CR—2000-209921/VOL. 2, September 2000.

[12] Broeren, A. P., and Bragg, M. B., "Effect of Airfoil Geometry on Performance with Simulated Intercycle Ice Accretions," *Journal of Aircraft*, Vol. 42, No. 1, 2005, pp. 121-130.

[13] Rayle, Jr., R. E., "An Investigation of the Influence of Orifice Geometry on Static Pressure Measurements," M.S. Thesis, Dept. of Mechanical Engineering, Massachusetts Institute of Technology, Cambridge, MA, 1949.

[14] Chue, S. H., "Pressure Probes for Fluid Measurement," *Progress in Aerospace Sciences*, Vol. 16, No. 2, 1975, pp. 147-223.

[15] Addy, Jr., H. E., and Chung, J. J., "A Wind Tunnel Study of Icing Effects on a Natural Laminar Flow Airfoil," AIAA Paper 2000-0095, 38th Aerospace Sciences Meeting and Exhibit, Reno, NV, Jan. 2000.

[16] Vickerman, M. B., Choo, Y. K., Schilling, H. W., Baez, M., Braun, D. C., and Cotton, B. J., "Toward an Efficient Icing CFD Process Using an Interactive Software Toolkit—SmaggIce 2D," AIAA Paper 2002-0380, 40th Aerospace Sciences Meeting and Exhibit, Reno, NV, Jan. 2002.

[17] Gurbacki, H. M., and Bragg, M. B., "Unsteady Aerodynamic Measurements on an Iced Airfoil," AIAA Paper 2002-0241, 40th Aerospace Sciences Meeting and Exhibit, Reno, NV, Jan. 2002.

[18] Broeren, A.P., Lee, S., LaMarre, C. M., and Bragg, M.B., "Effect of Airfoil Geometry on Performance with Simulated Ice Accretions Volume 1: Experimental Investigation," Report No. DOT/FAA/AR-03/64, August 2003.

[19] Papadakis, M. Alansatan, S. and Seltmann, M., "Experimental Study of Simulated Ice Shapes On a NACA 0011 Airfoil," AIAA Paper 99-0096, 37th Aerospace Sciences Meeting and Exhibit, Reno, NV, Jan. 1999.

[20] Broeren, A.P., "An Experimental Study of Unsteady Flow over Airfoils near Stall," Ph.D. Dissertation, Department of Mechanical Eng., Univ. of Illinois, Urbana, IL, 2000.

[21] Blumenthal, L.A., "Surface Pressure Measurement on a Three-Dimensional Ice Shape," M.S. Thesis, Dept. of Aerospace Engineering, Univ. of Illinois, Urbana, IL, 2005.

[22] Rae, W.H., and Pope, A., *Low-Speed Wind Tunnel Testing*, Wiley, New York, 1984, pp. 349-362.

[23] Kline, S.J., and McClintock, F.A., "Describing Uncertainties in Single-Sample Experiments," *Mechanical Engineering*, Vol. 75, Jan. 1953, pp. 3-8.

[24] Coleman, H.W., and Steele, W.G., *Experimentation and Uncertainty Analysis for Engineers*, John Wiley and Sons, New York, 1989, pp. 40-118.

[25] Mogili, P., Thompson, D. S., Choo, Y., and Addy, H., "RANS and DES Computations for a Wing with Ice Accretion," AIAA Paper 2005-1372, 43rd Aerospace Sciences Meeting and Exhibit, Reno, NV, Jan. 2005.

[26] Pan, J., and Loth, E., "Effect of Airfoil Geometry on Performance with Simulated Ice Accretions, Volume 2: Numerical Investigation," DOT/FAA/AR–3/65, Aug. 2003.

[27] Kim, H., "Effects of Leading-edge Ice Accretion Geometry on Airfoil Performance," M.S. Thesis, Dept. of Aerospace Engineering, Univ. of Illinois, Urbana, IL, 2004.

[28] Roberts, W., "Calculation of Laminar Separation Bubbles and Their Effect on Airfoil Performance," *AIAA Journal*, Vol. 18, No. 1, 1980.